Design and Research of a Self-Propelled Pipeline Robot Based on Force Analysis and Dynamic Simulation

Yan Gao[1], Jiliang Wang[2], Ming Cheng[1,3], Tianyun Huang[2]*

***Abstract*—In pipeline inspection, traditional tethered inspection robots are severely constrained by cable length and weight, which greatly limit their travel range and accessibility. To address these issues, this paper proposes a self-propelled pipeline robot design based on force analysis and dynamic simulation, with a specific focus on solving core challenges including vertical climbing failure and poor passability in T-branch pipes. Adopting a wheeled configuration and modular design, the robot prioritizes the core demand of body motion control. Specifically, 3D modeling of the robot was first completed using SolidWorks. Subsequently, the model was imported into ADAMS for dynamic simulation, which provided a basis for optimizing the drive module and motion control strategy. To verify the robot's dynamic performance, an experimental platform with acrylic pipes was constructed. Through adjusting its body posture to surmount obstacles and select directions, the robot has demonstrated its ability to stably traverse various complex pipeline scenarios. Notably, this work offers a technical feasibility reference for the application of pipeline robots in the inspection of medium and low-pressure urban gas pipelines.**

I. INTRODUCTION

Urban gas pipelines are the core infrastructure for urban energy supply. With the extension of their service life, safety hazards such as leakage, corrosion, and third-party construction damage to pipelines are becoming increasingly prominent, which can easily lead to gas leakage. Once such leakage accidents occur, they will directly threaten public safety and the ecological environment.

The existing gas leakage detection technology has obvious shortcomings. The commonly used methods for external detection include fiber optic leak detection [1], laser methane telemetry [2], and ground penetrating radar [3], which are easily affected by burial depth, pipe materials, and electrical properties of underground media, leading to deviation in leak point positioning or missed detection. In terms of internal inspection, high-pressure metal long-distance pipelines have widely used pipeline pig mounted magnetic leakage detection technology. However, the topology of medium and low-pressure urban combustion deep buried crossing pipelines is complex and the range of diameter changes is large. Existing internal inspection equipment is difficult to adapt to such conditions, and specialized products are still blank. Therefore, relevant internal inspection has become an urgent technical requirement in the industry.

The self-propelled pipeline robot is the core equipment to solve this problem, which needs to perform defect detection and autonomous movement based on perception technology in closed narrow pipelines [4]. However, existing pipeline robot often have problems such as complex structure, single adaptation to working conditions, and limited operating range due to wired drive [5]. In study [6], the modular in-pipe inspection robot MRINSPECT IV adopts a multi-module series structure and independent wheel drive. It was developed for inspecting 4-inch nominal inside diameter urban gas pipelines, addressing the issue of traditional wheeled robots getting stuck in bend pipes and T-branch pipes. In study [7], [8], [9], and [10], the snake like robots ACM-R series use flexible joints to improve the passability of curved pipes. The robots gradually iterate from basic snake like motion to active joint with active wheel, amphibious, track wheel combined with parallel linkage and other configurations. By increasing joint degrees of freedom and adapting to special motion parts, these robots can adapt to more scenarios. In study [11], [12], and [13], the wheeled pipeline robots AIRo series designed by professor Ma et al. are capable of efficiently addressing complex pipeline passability issues. The multi-unit configuration, passive elastic suspension design, and application of series elastic actuators enable these robots to stably pass through vertical pipes and T-shaped pipes. In study [14], a trailer type path drawing unit pulled by a pipeline inspection robot is proposed, which is only equipped with a low-cost internal measurement unit (IMU) and encoder for measuring the path of pipelines with a diameter of 3-4 inches. In study [15], researchers proposed a modular multi-unit wheeled pipeline robot to meet the internal inspection needs of urban low-pressure gas pipelines, overcoming the core technological limitations of traditional pipeline inspection gauge (PIG) detection equipment that relies on high-pressure fluid propulsion.

At present, most modular pipeline robots rely on wired power supply and data transmission [16], which makes it difficult to meet the long-distance operation needs of deep buried pipelines. As presented in Fig. 1, we focuses on the research of a wireless modular self-propelled pipeline robot for urban medium and low pressure gas pipelines, which overcomes the constraints caused by cables by using a self-propelled method with internal power supply for the robot. Firstly, use SolidWorks software for structural modeling, and then import the three-dimensional model into ADAMS software for dynamic simulation. By simulating the motion characteristics of pipeline robots in different scenarios such as

*Corresponding author: huangtianyun@pku.edu.cn

[1]Author is with the School of Mechanics and Engineering Science, Peking University, Beijing, China. Email: gloriagaohu@stu.pku.edu.cn (Yan Gao), Email: chengming@pku.edu.cn (Ming Cheng)

[2]Author is with the School of Advanced Manufacturing and Robotics, Peking University, Beijing, China. Email: wangjiliang@pku.edu.cn (Jiliang Wang), Email: huangtianyun@pku.edu.cn (Tian-Yun Huang).

[3]Author is with the Peking University Nanchang Innovation Institute, Nanchang, China. Email: chengming@pku.edu.cn (Ming Cheng).

straight pipes, bent pipes, variable diameters, and tees, optimize the structural parameters and motion control strategies of the robots. Finally, the passability and motion stability of the robot were verified through real pipeline experiments, and the adaptability of the pipeline robot to complex pipelines was studied.

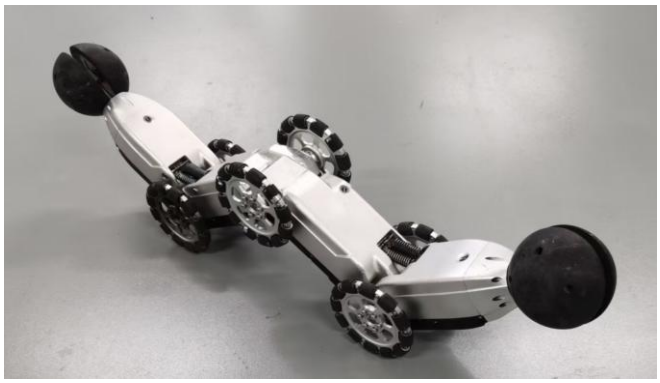

Fig. 1. Overview of the proposed self-propelled pipeline robot. The pipeline robot adopts wireless communication and internal battery power supply, with a range of 2 hours and a range of 1 kilometer. The robot is 0.92 m long, 0.15 m wide, 0.28 m high, and weighs approximately 10.04kg.

The rest of this paper is organized as follows. In Section II, the modular design and adaptive variable diameter methods of the robot are introduced. A dynamic simulation platform based on ADAMS is built in Section III. The robot's passability is verified through actual experiments in Section IV. Finally, conclusions are drawn in Section V.

II. Structural Design of Pipeline Robots

A. Scheme Selection

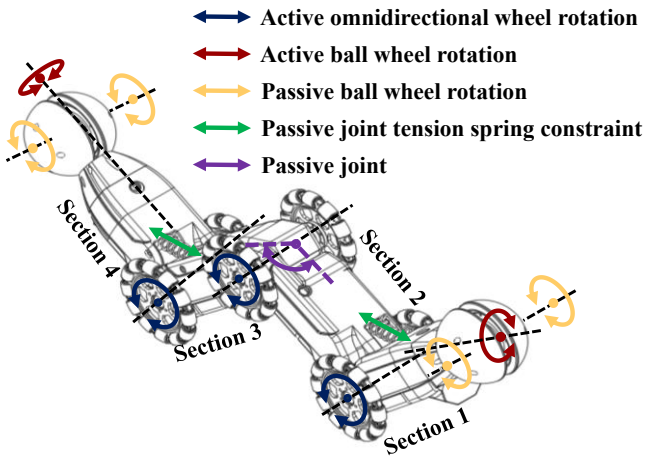

Fig. 2. Three-dimensional CAD model of the self-propelled in-pipe inspection robot.

As depicted in Fig. 2, the rotational motion of each joint of the self-propelled in-pipe inspection robot is illustrated. The pipeline robot adopts a modular design, with a four sections body and front and rear ball wheels, forming a W-shaped in-pipe robot. The robot has 12 degrees of freedom, including 5 active degrees of freedom and 7 passive degrees of freedom. Three of the active degrees of freedom are achieved by the motors inside the second and third sections of the robot body driving the omnidirectional wheels through the transmission module to achieve active rotation. The other two active degrees of freedom are achieved by the motors in the first and fourth sections driving the front and rear ball wheels to rotate around the axis of rotation. What's more, the robot has 6 omnidirectional wheels, each with 12 small rollers on its circumference, for a total of 72 local degrees of freedom. In order to maintain the robot in a W-shaped posture, joint angle limitation is required between each module. Among them, the first and second sections of the fuselage are passively constrained by tension springs, while the third and fourth sections are passively rotated. In study [17], the multi link pipeline inspection robot uses elastic actuators to achieve constraint and rotation between joints. In study [18], the middle joint of AIRo-2.3s adopts active torque control, which is achieved through a series of elastic actuators (SEA) for joint torque control and sensing. However, our developed self-propelled pipeline robot, due to the need to install batteries and communication modules internally, requires structural optimization each section can achieve active drive control in the internal space to achieve equivalent motion performance. In addition, both hemispheres of the front and rear ball wheels can passively rotate around the axis of the ball wheel, making it convenient for overcoming obstacles. Each section of the pipeline robot is equipped with a drive module, power supply module, control module, and wireless communication module inside the body, and each section can achieve realize drive control. It should be noted that due to the wireless cable driving method used in this robot, modular integration and reasonable spatial layout are required to ensure the endurance and driving performance of the robot, as well as sufficient wireless communication distance.

B. Force Analysis During Motion

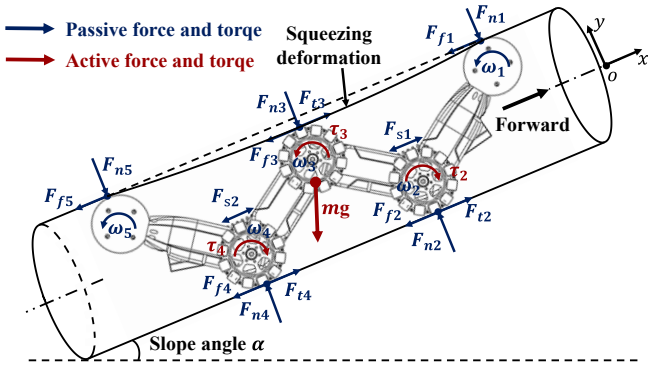

Fig. 3. The force analysis results of pipeline robots crawling in inclined and deformed pipelines.

As shown in Fig. 3, the force situation of the pipeline robot in an inclined and deformed pipeline is shown. It should be noted that there are two contact points between the pipe wall and the ith pair of omnidirectional wheels. In order to simplify the analysis of the resultant tangential force on the omnidirectional wheels here. During the process of slope movement, the motors of the second and third sections of the robot body drive three pairs of omnidirectional wheels to rotate, exerting torques of τ_1, τ_2, and τ_3. The ball wheel and roller will encounter frictional resistance from the pipe wall during their rotation along the wall. It should be noted that the front and rear ball wheels rotate passively, while the three pairs of omnidirectional wheels in the middle rotate actively. Under

the tension of the front and rear tension springs, the ball wheels and omnidirectional wheels of the pipeline robot can tightly adhere to the pipe wall. The vertical pressure exerted by the pipe wall on the ball wheel and roller is F_{ni}. In a pipeline with an inclination angle of α, the pipeline robot moves forward at a constant speed along the pipeline, and needs to satisfy the following relationship in the x direction as follows.

$$\sum_{i=2}^{4} F_{ti} - \sum_{i=1}^{5} F_{fi} = \mathrm{m} \cdot \mathrm{g} \cdot \sin\alpha + \mathrm{m} \cdot a \tag{1}$$

where, F_{ti} is the tangential force exerted by the pipeline on the i th pair of omnidirectional wheels, F_{fi} is the rolling resistance exerted by the pipe wall on the ball wheel and roller during rotation, m is the mass of the pipeline robot, g is the local gravitational acceleration constant, and a is the acceleration of the pipeline robot in the direction of advancing along the pipeline axis.

In addition, during the forward movement of the robot, the rolling resistance experienced by the i th pair of omnidirectional wheels can be given by

$$F_{fi} = \delta \cdot F_{ni} \tag{2}$$

where, δ is the rolling resistance coefficient. Assuming there is no slippage between the roller and the pipe wall, the tangential force is calculated as

$$F_{ti} = \frac{\tau_i}{r_i} \tag{3}$$

where, τ_i is the driving torque of the motor driving the omnidirectional wheels to rotate, and r_i is the radius of the omnidirectional wheel, and the values of i are 2, 3, and 4. The force analysis in the y direction needs to meet the following requirements.

$$\sum_{i=1}^{5} F_{ni} = \mathrm{m} \cdot \mathrm{g} \cdot \cos\alpha \tag{4}$$

where, α is the inclination angle of pipeline mentioned earlier. The force of the front and rear linear tension spring between the bodies of the pipeline robot can be calculated as follows

$$F_{\mathrm{sj}} = \mathrm{k_j} \cdot \Delta s_{\mathrm{j}} \tag{5}$$

where, the values of j are 1 and 2. $\mathrm{k_j}$ denotes the stiffness of the front and rear linear spring, and Δs_{j} represents the deformation amount of the front and rear linear springs.

Fig. 4 displays the vertical pressure force analysis along the circumference of the pipeline when the pipeline robot climbs inside the inclined pipeline, showing the normal pressure distribution and force balance relationship between the robot and the inner wall of the pipeline.

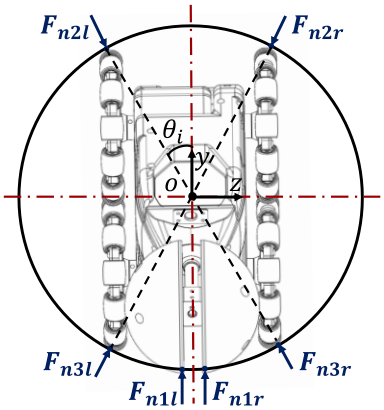

Fig. 4. Analysis of vertical pressure force along the circumference of the pipeline when the pipeline robot climbs in an inclined pipe.

Regarding the front and rear ball wheels, the vertical pressure along the y-direction is given as

$$F_{ni} = F_{nil} + F_{nir} \tag{6}$$

where, the values of i are 1, and 5. With regard to the three pairs of omnidirectional wheels in the middle, the vertical pressure along the y-direction can be defined by

$$F_{ni} = F_{nil} \cdot \cos\theta_i + F_{nir} \cdot \cos\theta_i \tag{7}$$

where, the values of i are 2, 3, and 4. θ_i is the angle between the line connecting the contact point of the i th pair of omnidirectional wheels to the center of the circle and the vertical direction of the robot body.

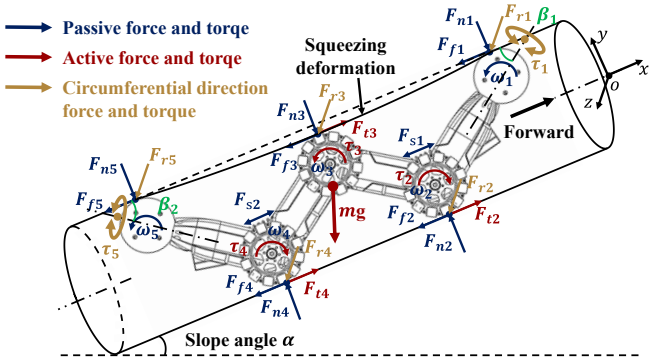

Fig. 5. The force analysis results of the pipeline robot adjusting its posture while crawling and rotating the ball wheel in inclined and deformed pipelines. The circumferential direction force and torque in the figure are the ones that need to be added when the pipeline robot rotates around the pipeline axis.

As depicted in Fig. 5, the robot moves forward while rotating the ball wheel to adjust its posture in inclined and deformed pipelines. At this point, the force balance

relationship along the circumference of the pipeline can be denoted as

$$\tau_1 \cdot \sin\beta_1 + \tau_5 \cdot \sin\beta_2 + \sum_{i=1}^{5} F_{ri} \cdot r_{pi} = \mathrm{m} \cdot \xi \qquad (8)$$

where, β_1 and β_2 are the angles between the axis directions of the front and rear ball wheels and the pipe wall, respectively. τ_1 and τ_5 are the torque of the front and rear ball wheels rotating, respectively. F_{ri} is the circumferential resistance applied by the pipe wall to the roller in the circumferential direction, and r_{pi} is the radial distance from the ith contact point between the robot and the pipe wall to the pipeline axis. ξ is the angular acceleration of the robot along the axis direction, which can be calculated as follows

$$\xi = \frac{dw_c}{dt} \qquad (9)$$

where, w_c is the angular velocity of the robot along the pipeline axis direction.

Note that this section presents the force analysis of the pipeline robot along the slope direction. When the slope angle is 0°, this corresponds to the force analysis in the horizontal pipeline scenario. When the slope angle is 90°, this refers to the force analysis for the robot working in the vertical pipeline scenario. Following the theoretical analysis, we will next establish a model in the ADAMS simulation software and perform dynamic simulations, to verify the passability and dynamic performance of the self-propelled pipeline robot.

III. Dynamics Simulation of Pipeline Robot Based on ADAMS

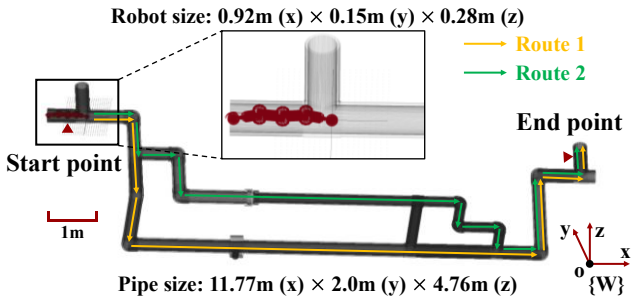

Fig. 6. Two forward route of pipeline robot based on ADAMS simulation in complex three-dimensional pipelines.

The overwiew of our simulation scenario is shown in Fig. 6, this is a simulation environment constructed using ADAMS software, tailored to replicate real-world gas pipeline scenarios. During the simulation process, it is necessary to construct a simulated pipeline environment, define the collision and contact properties between the robot and the pipe wall, and create the robot's active force, torque, and passive constraints. Appropriate model simplification is required during the model establishment and dynamic analysis in ADAMS software. In addition, the core function of this simulation scenario is to reproduce the path environment of real gas pipelines and verify the key performance of pipeline robots such as traversal capability and motion stability under different routes.

In the world coordinate system {W} of the simulation scene, the gas pipeline's dimensions along the x, y, and z directions are 11.7 m, 2.0 m, and 4.76 m, respectively. This simulation configuration replicates the spatial layout of actual natural gas pipelines in a 1:1 ratio. The pipeline robot has dimensions of 0.92 m, 0.15 m, and 0.28 m along the x, y, and z directions respectively. Two motion routes are designed in this scenario, route 1 marked in yellow and route 2 marked in green. The robot starts from the starting point on the left side of the diagram, moves along its designated route, and finally reaches the endpoint on the right side of the diagram.

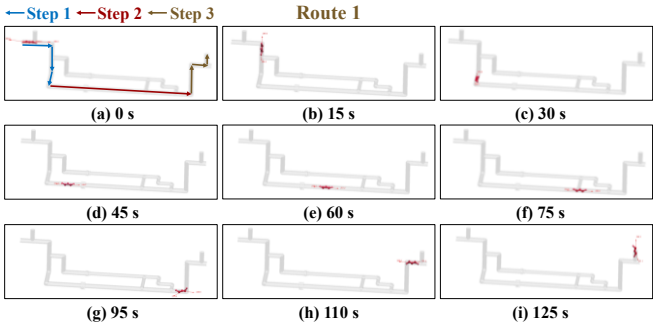

Fig. 7. The motion of the self-propelled pipeline robots in the scenario of route 1.

Fig. 7. exhibits the dynamic motion process of the pipeline robot along route 1, while Fig. 7(a) depicts the three stages of the pipeline robot's motion along route 1. Stage 1, as shown by the blue line in Fig. 7(a), involves the robot passing through three consecutive bends. In Stage 2, the robot advances in a straight line, as shown by the red path line in Fig. 7(a). In Stage 3, the robot continuously passes three bends and finally reaches the endpoint position, as shown by the yellow line in the figure. Fig. 7(a) to Fig. 7(i) record the spatial positions of key time nodes during the robot's crossing of route 1. Starting from the initial position of 0 s, corresponding to the left starting point of the simulated scene, the robot passes through various pipeline segments at each stage, including straight pipes, bent pipes, variable diameter pipes, and T-branch pipes. After a continuous motion process, the pipeline robot reached the right endpoint in 125 s, completing the complete crossing of route 1 and verifying the stability and passability of the pipeline robot's motion in route 1.

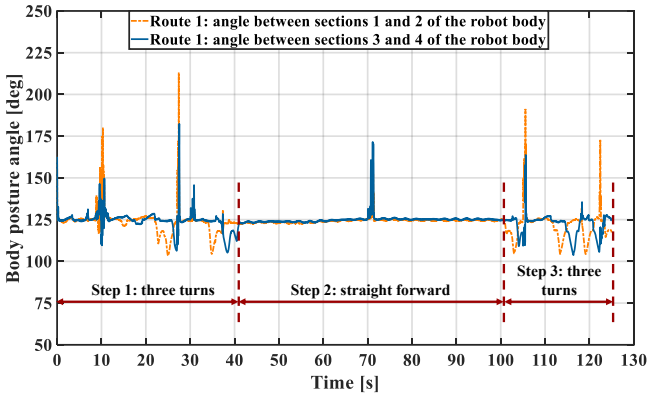

Fig. 8. The variation of the body posture angle of the pipeline robot in the scenario of route 1.

As depicted in Fig. 8, this picture shows the variation of the pipeline robot's body posture angle along route 1. The orange dotted line represents the variation of the angle between the sections 1 and 2 of the body over time, while the blue solid line represents that of the angle between the sections 3 and 4 of the body over time. In Stage 1, the robot passes through 2 bends and 1 tee pipe, and the variation trend of the angle between sections 3 and 4 of the body is similar to that between sections 1 and 2 of the body, but with a time lag. In Stage 2, the robot advances in a straight line. At approximately 72 s, due to the need to adjust the body posture, it changes from a lateral to a forward direction, causing a sudden change in the robot's body posture angle. In Stage 3, the robot takes three turns and finally reaches the final position.

In Fig. 9, this graph illustrates the temporal variation of the pipeline robot's front and rear spring tension, which is similar to the trend of the body attitude angle over time described in Fig. 8. It should be noted that to maintain a W-shaped posture during the robot's movement, the tension springs between the first and second sections of the body and between the third and fourth sections need to have a certain amount of tension, ensuring close contact between the ball wheels, omnidirectional wheels, and the upper and lower pipe walls. During the movement of the robot in straight pipelines, the tension is maintained at approximately 250 N, while the joint angle of the body is maintained at around 125 degrees. When the attitude angle of the first and second sections of the fuselage increases, the deformation of springs increases and the tension rises. The trend of the absolute value of the tension is consistent with that of the fuselage attitude angle revealed in Fig. 8.

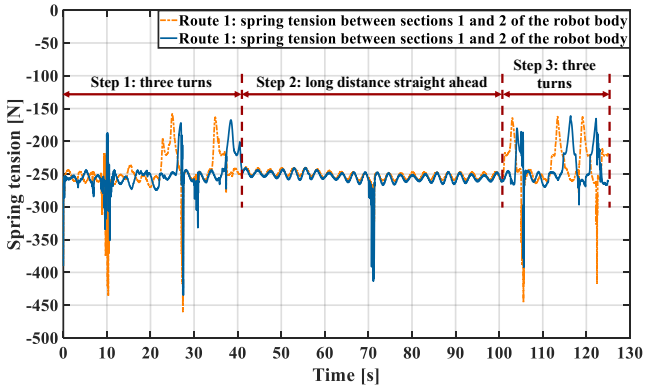

Fig. 9. In the scenario of route 1, the changes in the tension of the front and rear springs of the pipeline robot.

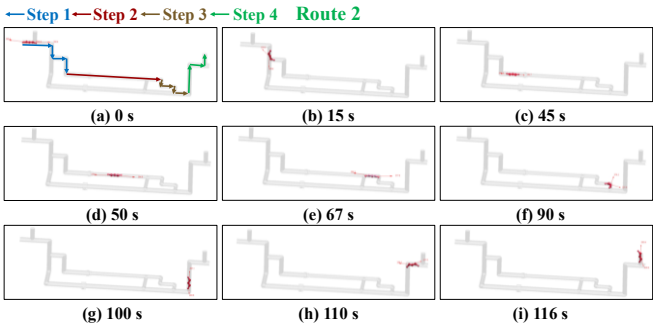

Fig. 10. The motion of the self-propelled pipeline robots in the scenario of route 2.

Fig. 10 showcases the motion process of the pipeline robot along route 2. Route 2 involves more turns than route 1. As illustrated in Fig. 10(a), this motion can be divided into four steps. The robot starts from the initial point at 0 s, traverses pipeline segments across four steps, and finally reaches the endpoint at 116 s, verifying its motion stability and passability. In the first step, the robot passes through 3 bends and 1 tee pipe; it then moves in a straight line in step 2. In step 3, the robot traverses 3 bends and 1 tee pipe, and in the last step, it passes through 2 bends and 1 tee pipe.

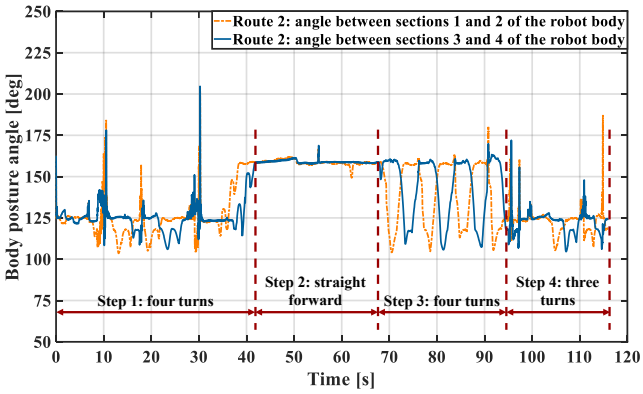

Fig. 11. The variation of the body posture angle of the pipeline robot in the scenario of route 2.

Fig. 11 displays the variation of the body posture angle of the pipeline robot over time in route 2. It should be noted that the robot needs to adjust its body posture before bending, so that the W-shaped side of the pipeline robot conforms to the bending direction of the pipeline. In the first stage, the time is about 0 to 42 s, and the angle between the two sections of the fuselage fluctuates significantly at the bend. Step 2 is about 42 to 67 s, and the robot's body posture angle is relatively stable when moving in a straight line. Step 3 is approximately 67 to 94 s, and step 4 is approximately 94 to 116 s. When the robot passes through bends, the posture angle of the robot body fluctuates frequently with posture adjustment, which intuitively reflects its posture adaptation process under the complex working conditions of route 2.

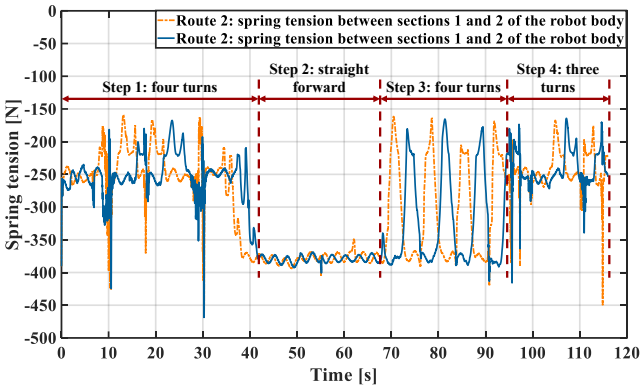

Fig. 12. In the scenario of route 2, the changes in the tension of the front and rear springs of the pipeline robot.

Fig. 12 exhibits the time variation of the tension of the front and rear springs of the pipeline robot in the scenario of route 2. The orange dotted line and the blue solid line correspond to the tension of the front and rear springs of the machine body, respectively. The tension variation of the spring is directly linked to the complex working conditions of route 2. In step 1, the robot needs to frequently adjust its body posture to adapt to bends, resulting in increased spring deformation and significant fluctuations in tension. In step 2, the body posture is stable, the spring has no external shape change, and the tension remains stable. The slight jump that occurs is due to adjusting the body posture angle of the robot to facilitate cornering. In subsequent steps 3 and 4, the robot enters the multi curve area again, and the body posture is repeatedly adjusted to drive frequent changes in spring deformation, and the tension continues to fluctuate. This dynamic change in tension is a manifestation of pipeline robots adapting to complex pipeline environments. By adjusting the tension in real-time, the robot is ensured to maintain reliable contact with the pipe wall in various pipe sections, thereby providing sufficient driving force.

IV. Experimental Verification

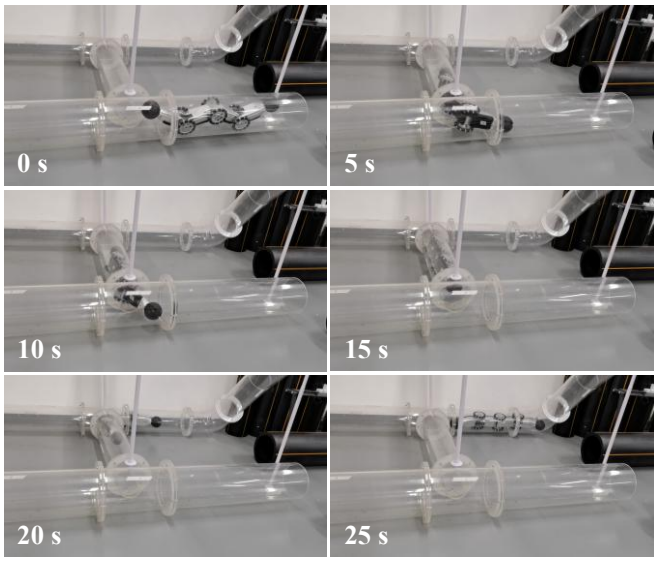

Fig. 13. The motion of a self-propelled pipeline robot through two T-branch pipes on a horizontal plane.

We have verified the passability and bending performance of the proposed self-propelled pipeline robot through theoretical force analysis and dynamic simulation. To further validate, we developed a self-propelled pipeline robot and tested its through ability in real pipeline scenarios. We established a complex pipeline environment with a diameter range of 200-250 mm to test the robot's passing performance. Fig. 13 displays the motion process of the self-propelled pipeline robot through two T-branch pipes in a horizontal plane, presenting the robot's travel status at time nodes of 0 s, 5 s, 10 s, 15 s, 20 s, and 25 s. The front and rear ball wheels of the robot serve as guidance, rotating around the pipeline axis to facilitate path direction selection and control of the forward direction. The three pairs of omnidirectional wheels in the middle of the robot serve as driving wheels, controlling the direction of the robot's movement based on the different contact points between the wheels and the pipeline, as well as the rotation direction of the wheels. During the 0-5 s process, the robot adjusts its body posture from a W-shaped upright position to a right side bending posture. It should be noted that the time is approximately around 5 s, due to change in the contact point between the omnidirectional wheel and the pipe wall, the rotation direction of the pair of omnidirectional wheels behind the robot needs to be reversed to provide forward driving force. What's more, the robot successfully passed through the first T-branch pipes, and following this strategy, the robot successfully passed through the second T-branch pipes. Throughout the process, the robot relied on motion control strategies to achieve attitude adjustment and continuous motion in the horizontal complex T-branch pipes, demonstrating its efficient throughput performance.

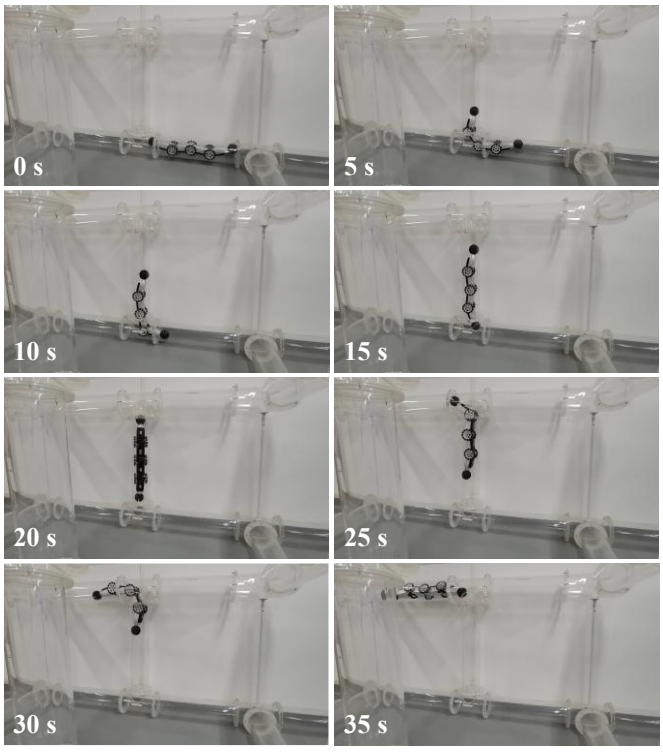

Fig. 14. The motion of a self-propelled pipeline robot climbing through two T-branch pipes on a vertical plane.

However, in a vertical plane, a robot needs to overcome its own gravity to climb vertically through T-junctions, which is

currently a technical challenge. Fig. 14 shows a screenshot of our pipeline robot passing through two three-way pipelines in the vertical direction. At around 10 s, if the pressure between the robot's omnidirectional wheels and the pipe wall is insufficient, slippage may occur. At this time, it is necessary to adjust the robot's posture by rotating the ball wheel to reduce slippage between the omnidirectional wheel and the pipe wall. During the process of 15 to 25 s, the robot adjusts its posture and selects the desired forward direction by rotating the ball wheel, demonstrating the flexibility of robot motion control and forward direction selection. During the process of 30 to 35 s, it should be noted that, similar to the situation of passing through the tee horizontally earlier, the contact position between our third pair of omnidirectional wheels and the pipe wall has changed. It is necessary to adjust the rotation direction of the omnidirectional wheels at the back to facilitate passing through the vertical tee pipe. Finally, the robot successfully passed through two T-branch pipes in a vertical plane.

V. Conclusions

In this study, we designed and developed a self-propelled pipeline robot, aiming to address the limitations of traditional wired robots and the challenge of traversing complex pipelines. By analyzing the force situation of the pipeline robot in the pipeline, the robot successfully passed through two complex pipeline routes in ADAMS simulation, verifying the effectiveness of the robot's motion control strategy in complex pipeline scenarios. Experiments further confirm that the robot can smoothly pass through horizontal and vertical T-branch pipes, fully demonstrating its excellent ability to pass through complex pipelines and providing reliable technical support for the detection of medium and low pressure gas pipelines.

In the future, we will focus on researching simultaneous localization and mapping (SLAM) and pipeline positioning technologies, laying a technical foundation for the autonomous navigation and movement of robots in actual gas pipeline scenarios.

Acknowledgment

The authors acknowledge with thanks the dedicated Adams simulation technical assistance provided by researcher Chengkai Wang of Hexagon Group. The authors thank the support of DeepCavas (Beijing) Technology Co., Ltd. in designing and manufacturing the robot.

References

[1] P. Thodi, M. Paulin, L. Forster, J. Burke, and G. Lanan, "Arctic pipeline leak detection using fiber optic cable distributed sensing systems," in Proc. OTC Arctic Technol. Conf., Houston, TX, USA, 2014, pp. OTC-24589.

[2] B. J. Smith, G. John, L. E. Christensen, and Y. Chen, "Fugitive methane leak detection using sUAS and miniature laser spectrometer payload: System, application and ground truthing tests," in Proc. IEEE Int. Conf. Unmanned Aircraft Syst. (ICUAS), Miami, FL, USA, 2017, pp. 369-374.

[3] H. Li, C. Chou, L. Fan, B. Li, D. Wang, and D. Song, "Toward automatic subsurface pipeline mapping by fusing a ground-penetrating radar and a camera," IEEE Trans. Autom. Sci. Eng., vol. 17, no. 2, pp. 722-734, 2019.

[4] R. Rayhana, H. Yun, Z. Liu, and X. Kong, "Automated defect-detection system for water pipelines based on CCTV inspection videos of autonomous robotic platforms," IEEE/ASME Trans. Mechatron., vol. 29, no. 3, pp. 2021-2031, 2023.

[5] A. Verma, A. Kaiwart, N. D. Dubey, F. Naseer, and S. Pradhan, "A review on various types of in-pipe inspection robot," Materials Today: Proc., vol. 50, pp. 1425-1434, 2022.

[6] S.-G. Roh and H. R. Choi, "Differential-drive in-pipe robot for moving inside urban gas pipelines," IEEE Trans. Robot., vol. 21, no. 1, pp. 1-17, Feb. 2005.

[7] S. Hirose and E. F. Fukushima, "Snakes and strings: New robotic components for rescue operations," Int. J. Robotics Res., vol. 23, no. 4-5, pp. 341-349, 2004.

[8] S. Hirose and H. Yamada, "Snake-like robots [tutorial]," IEEE Robotics Autom. Mag., vol. 16, no. 1, pp. 88-98, 2009.

[9] T. Ohashi, H. Yamada, and S. Hirose, "Loop forming snake-like robot ACM-R7 and its serpenoid oval control," in Proc. IEEE/RSJ Int. Conf. Intell. Robots Syst. (IROS), Taipei, Taiwan, 2010, pp. 413-418.

[10] H. Yamada, S. Takaoka, and S. Hirose, "A snake-like robot for real-world inspection applications (the design and control of a practical active cord mechanism)," Adv. Robotics, vol. 27, no. 1, pp. 47-60, 2013.

[11] A. Kakogawa and S. Ma, "Design of a multilink-articulated wheeled inspection robot for winding pipelines: AIRo-II," in Proc. IEEE/RSJ Int. Conf. Intell. Robots Syst. (IROS), Daejeon, South Korea, 2016, pp. 2115-2121.

[12] A. Kakogawa and S. Ma, "A multi-link in-pipe inspection robot composed of active and passive compliant joints," in Proc. IEEE/RSJ Int. Conf. Intell. Robots Syst. (IROS), Las Vegas, NV, USA, 2020, pp. 6472-6478.

[13] Y. Oka, A. Kakogawa, Y. Tian, and S. Ma, "Control technique of a V-shaped in-pipe robot composed of two underactuated roll-pitch joints," Adv. Robotics, vol. 36, no. 4, pp. 205-216, 2022.

[14] C. Hirose, S. Ota, A. Kakogawa, and S. Ma, "A pipeline route drawing system equipped with a towed unit using only low cost internal sensors," IEEE Trans. Ind. Electron., 2024.

[15] P. Chang, M. Wang, Z. Shao, A. Maimaiti, and W. Zhou, "Modular design of multi-unit pipeline inspection robot for low pressure gas pipeline," in Proc. 10th Int. Conf. Autom. Control Robotics Eng. (CACRE), Singapore, 2025, pp. 370-375.

[16] K. Murata, M. Kusumegi, A. Kakogawa, and S. Ma, "Elastic material selection for omni-wheels of in-pipe robots with high traction capability," Adv. Robotics, vol. 38, no. 13, pp. 896–905, 2024.

[17] A. Kakogawa and S. Ma, "Differential elastic joint for multi-linked pipeline inspection robots," in Proc. IEEE/RSJ Int. Conf. Intell. Robots Syst., Madrid, Spain, 2018, pp. 949-954.

[18] A. Kakogawa and S. Ma, "An in-pipe inspection module with an omnidirectional bent-pipe self-adaptation mechanism using a joint torque control," in Proc. IEEE/RSJ Int. Conf. Intell. Robots Syst., Macau, China, 2019, pp. 4347-4352.